Supporting information

Characterizing Carbon Ring-C_3N_4 Nanosheets as a Light Harvesting and Charge Carrier Transfer Agent: Photodegradation of Methylene Blue and Photoconversion of CO_2 to CH_4 as Case Studies

Hossein Ashrafi, Morteza Akhond, Maryam Zare, and Ghodratollah Absalan*,
Professor Massoumi Laboratory, Department of Chemistry, Shiraz University, Shiraz 71454, Iran
*gubsulun@yahoo.com; absalan@shirazu.ac.ir

Photocatalytic reduction of CO_2

Photocatalytic activity of the synthesized catalysts for CO_2 reduction was evaluated in a batch circulation water reactor (Pyrex tubular reactor) with a 300W Xe lamp as the light source. The reactor was double-walled for circulating water between these walls to maintain the solution at around 25°C. An amount of 40 mg photocatalyst powder and 100 mL H_2O were placed in the reactor. Then, the mixture was stirred under strong magnetic force for 10 min to homogenize the solution. The CO_2 (99.999%) gas was purged into the reactor for 40 min to saturate water with CO_2 and remove the dissolved air. After irradiation, the gas phase products were taken from the reactor in every 1 h by using a 1-mL Hamilton gas tight syringe to analyze it by gas chromatography equipped with flame ionisation detector. The isotope-labeled examination was carry out by gas chromatography-mass spectrometry (GC-MS, 7890A and 5875C, Agilent).

Electrochemical measurements

Electrochemical measurements were performed by a PGSTAT302N (Metrohm Autolab B.V., Utrecht, The Netherlands). The electrochemical cell was assembled with a conventional three-electrode system. The working electrodes were prepared by using samples coated on FTO glass. A saturated Ag/AgCl (saturated KCl) and a platinum wire were used as reference and auxiliary

electrodes, respectively. The electrolyte was Na_2SO_4 solution (0.5 mol L^{-1}) and the solution was purged with argon for 1h to remove O_2 before light irradiation. Electrochemical impedance spectroscopy (EIS) was performed using 5 mmol L^{-1} $K_3[Fe(CN)_6]/K_4[Fe(CN)_6]$ solution as the reversible redox probe with 0.1 mol L^{-1} KCl as the electrolyte.

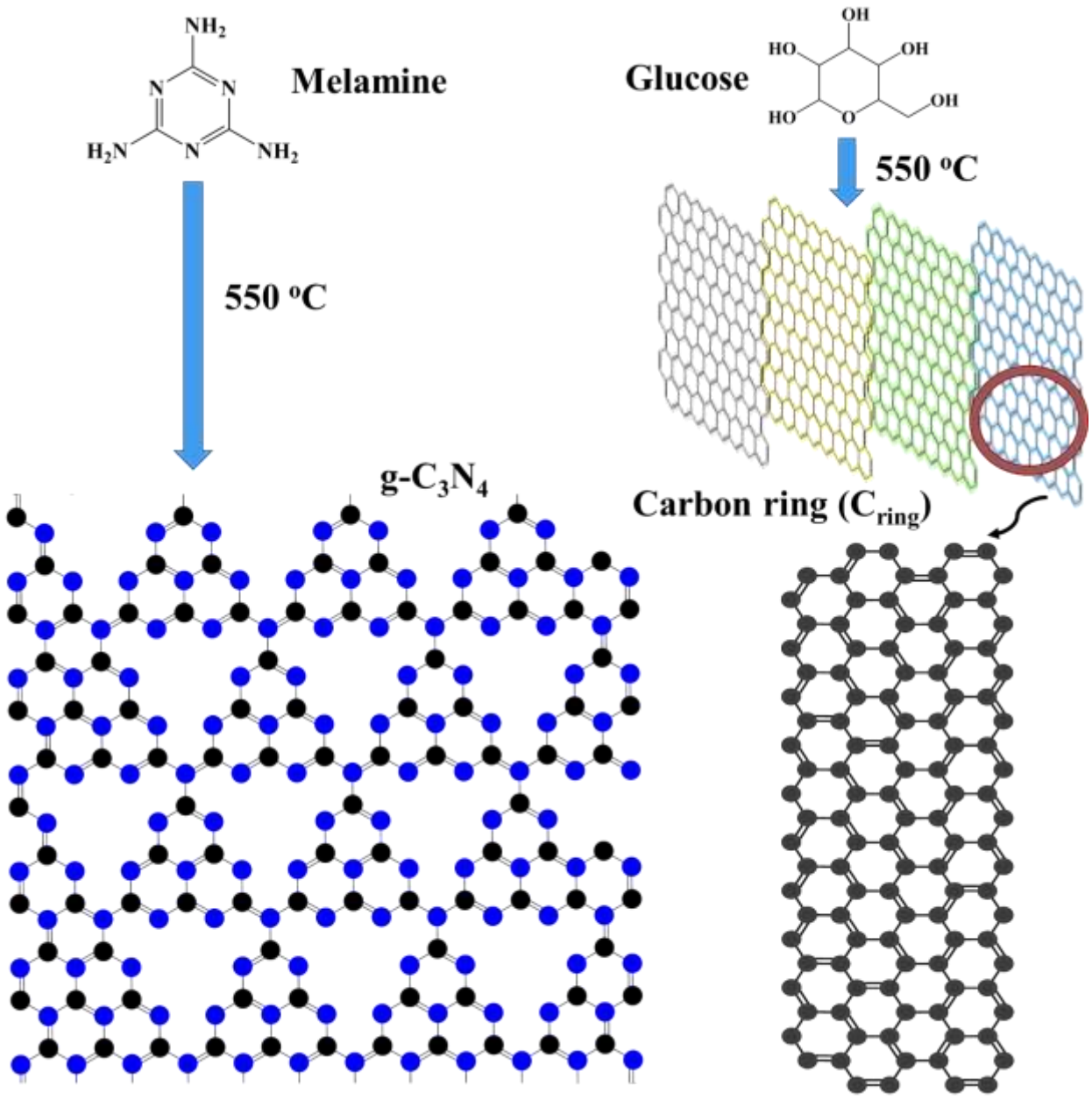

Figure S1. When glucose and melamine are heated to high temperatures, carbon and tri-s-triazine rings produce having sp^2 hybrid (two-dimensional domains in-plane with a similar aromatic structure).

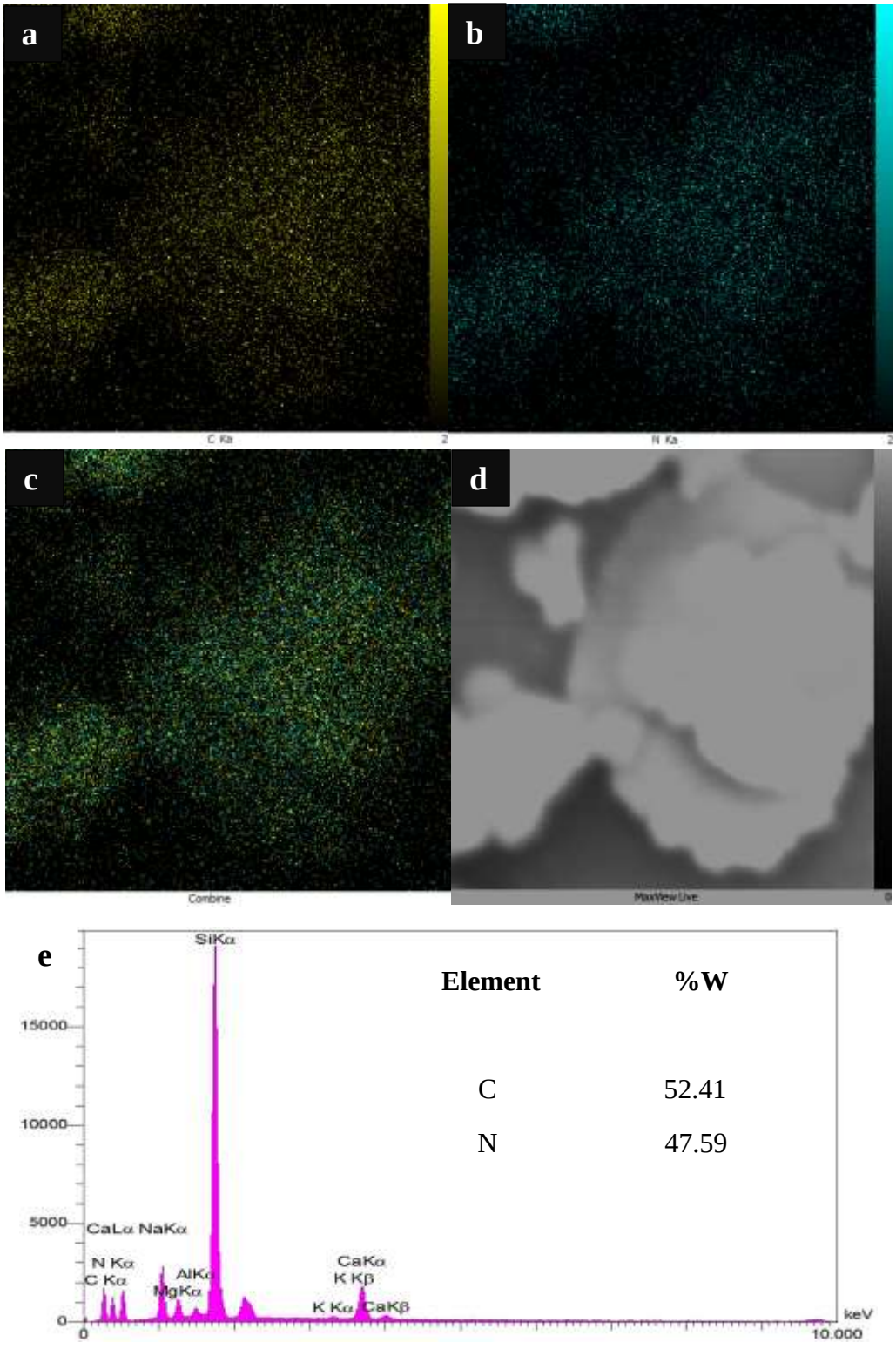

Figure S2. The SEM-EDS mapping images and spectra of C_{ring}-C_3N_4. (**a**), the C mapping image; (**b**), the N mapping image; (**c**), the combined C and N mapping image; (**d**), the SEM image shows the corresponding region for mapping; and (**e**), the EDS spectra of C_{ring}-C_3N_4.

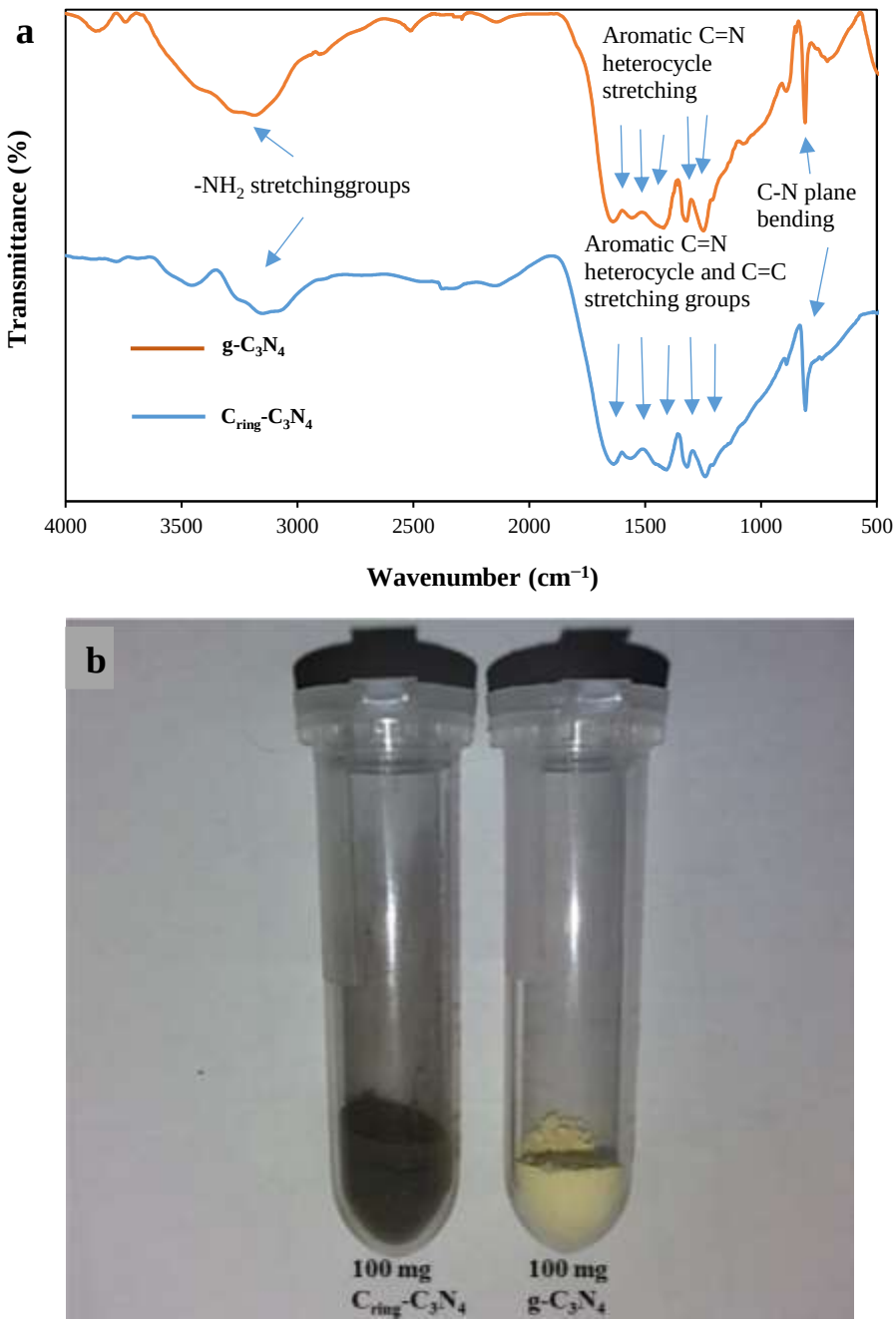

Figure S3. (**a**), the FT-IR spectra of C_{ring}-C_3N_4 and bulk g-C_3N_4. (b), Comparison between color of C_{ring}-C_3N_4 and bulk g-C_3N_4.

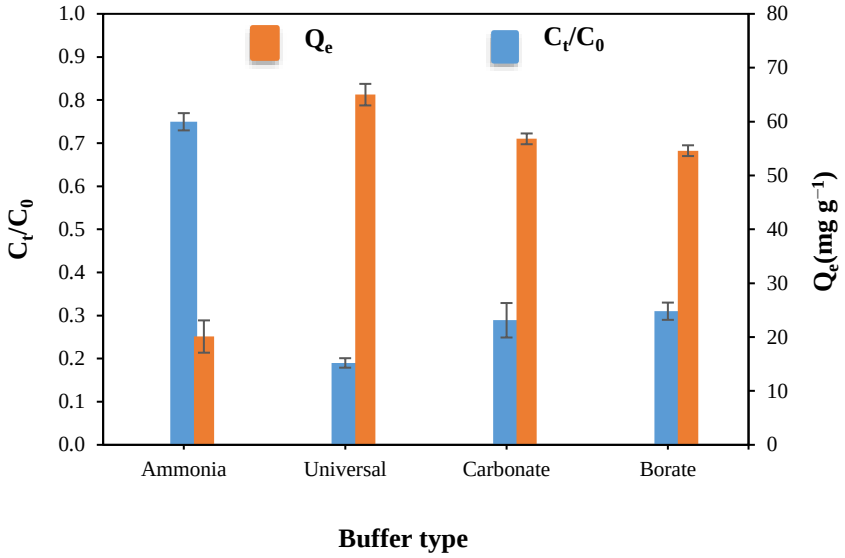

Figure S4. Effect of buffer type. Experimental conditions: 40.0 mL of 20.0 mg L^{-1} MB, 4.0 mg of C_{ring}-C_3N_4 with 0.01 mol L^{-1} universal buffer at pH=11.0.

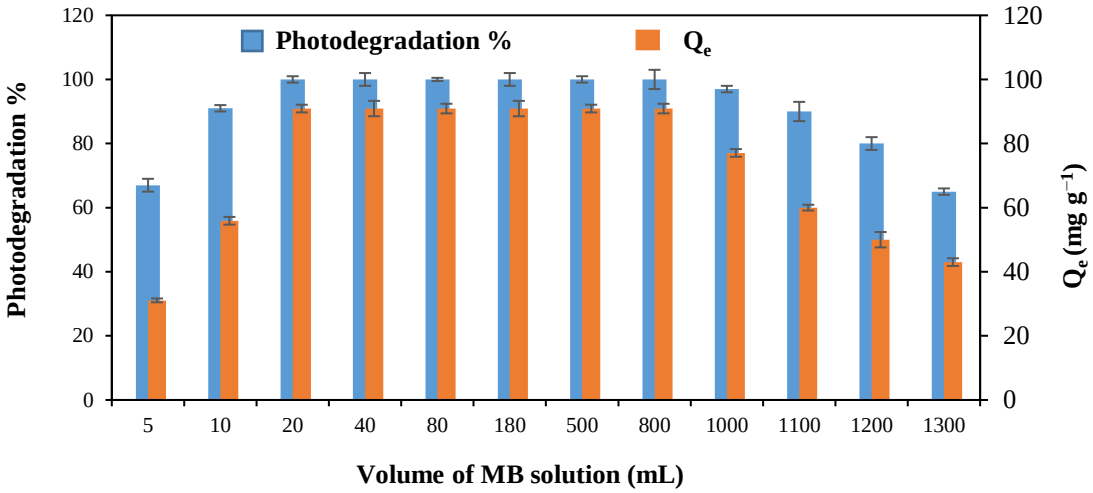

Figure S5. Breakthrough volume in adsorption/photodegradation of MB.

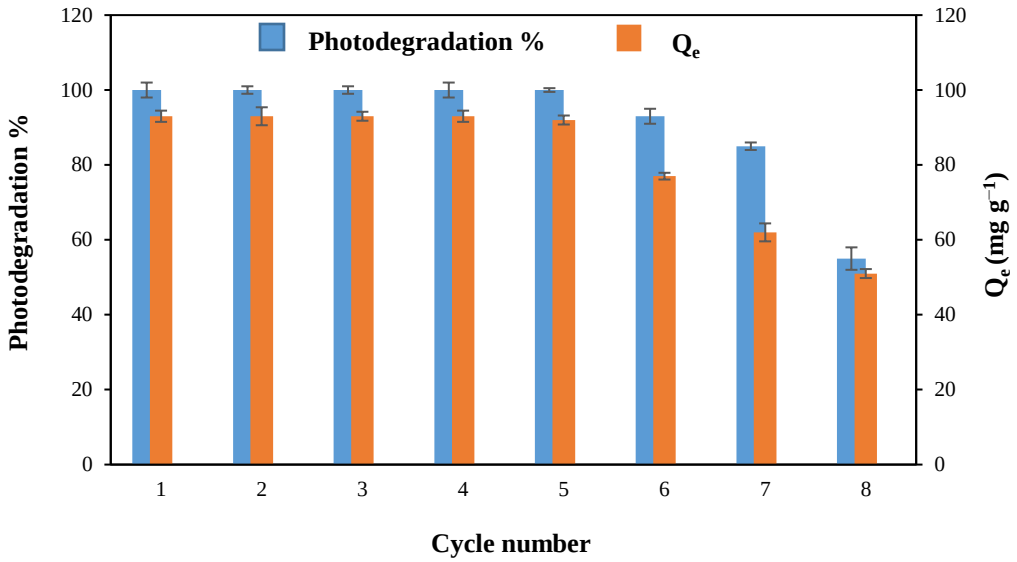

Figure S6. Reusability of the photocatalysts in several successive processes in the adsorption/photodegradation of MB.

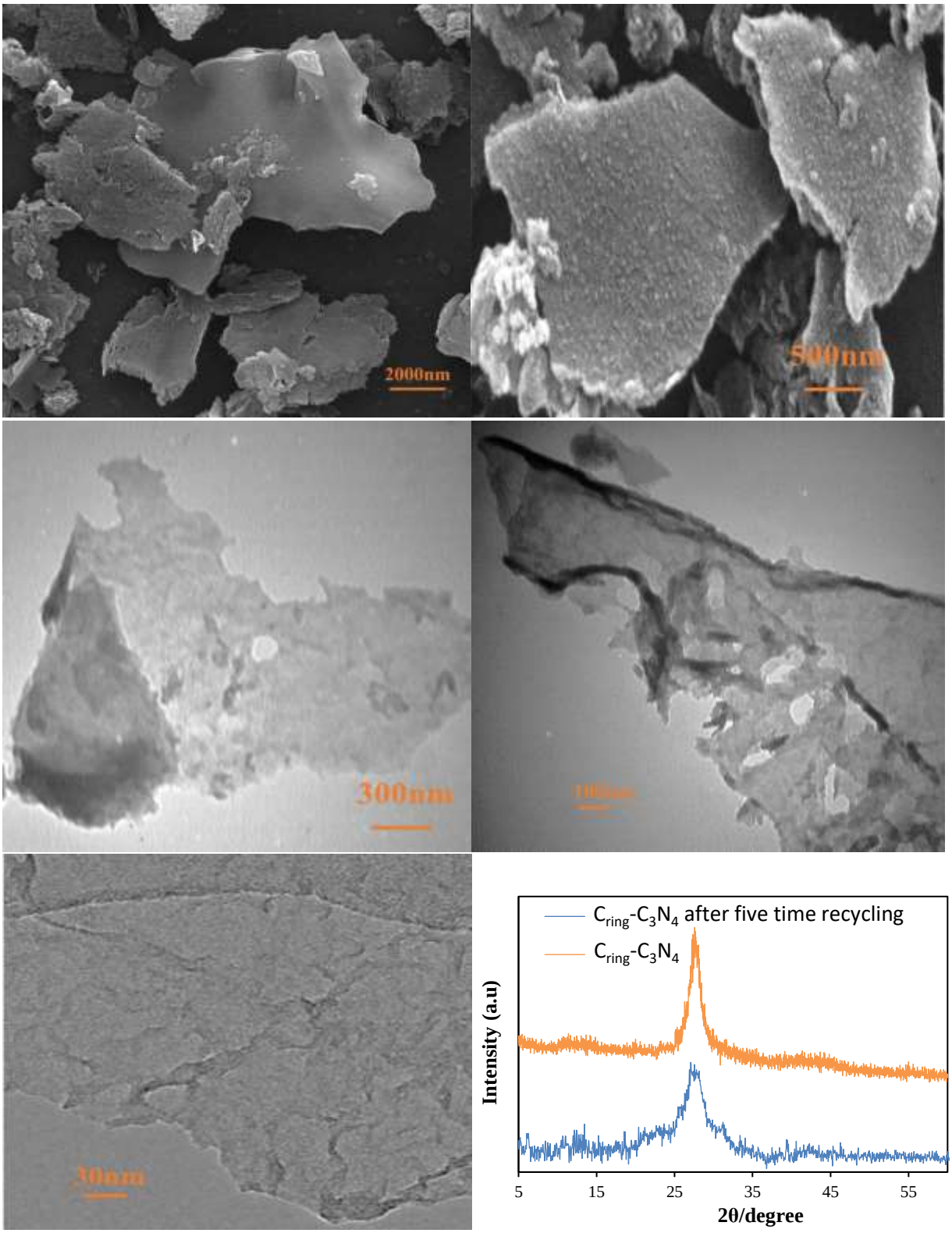

Figure S7. SEM, TEM, and XRD analyses after 5-time usage of C_{ring}-C_3N_4 photocatalyst.

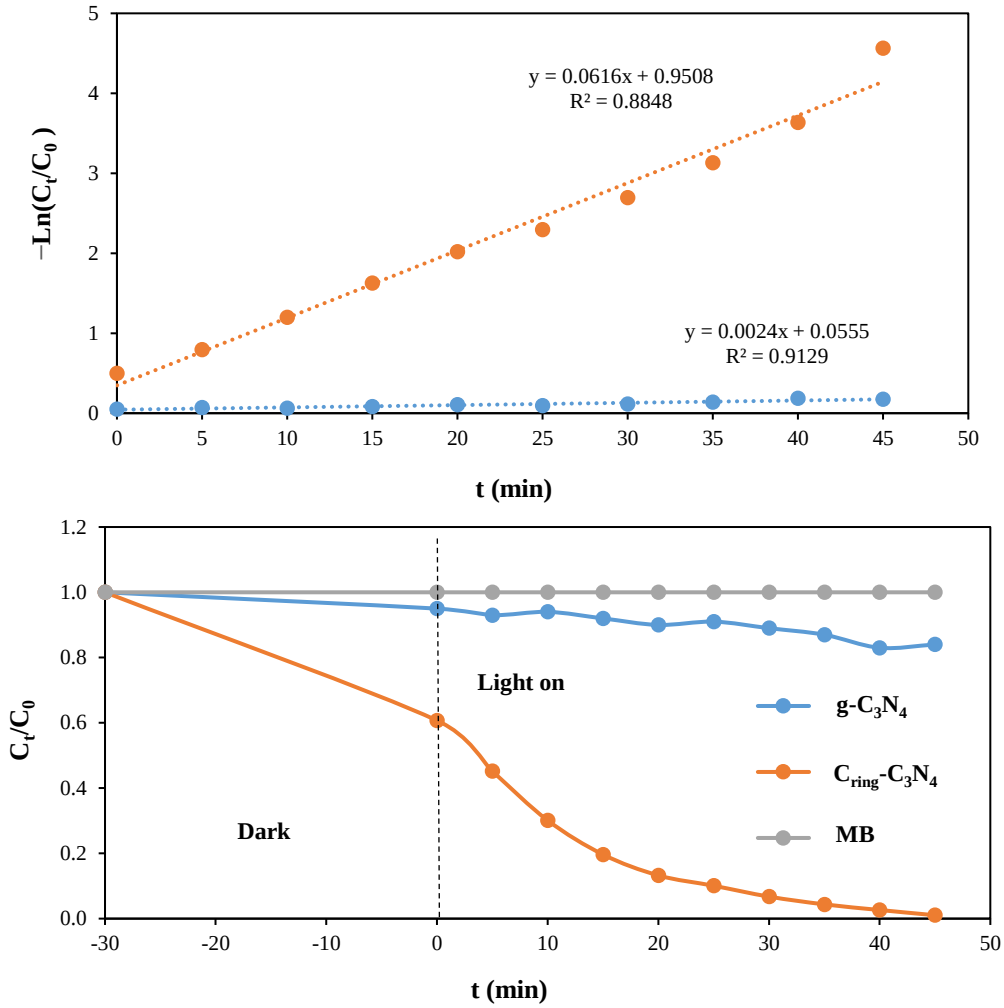

Figure S8. The kinetic simulation curves of MB photodegradation under visible light irradiation. Experimental conditions: 4.0 mg C_{ring}-C_3N_4, 40.0 mL of 20.0 mg L^{-1} MB with 0.05 M universal buffer at pH=11.0).

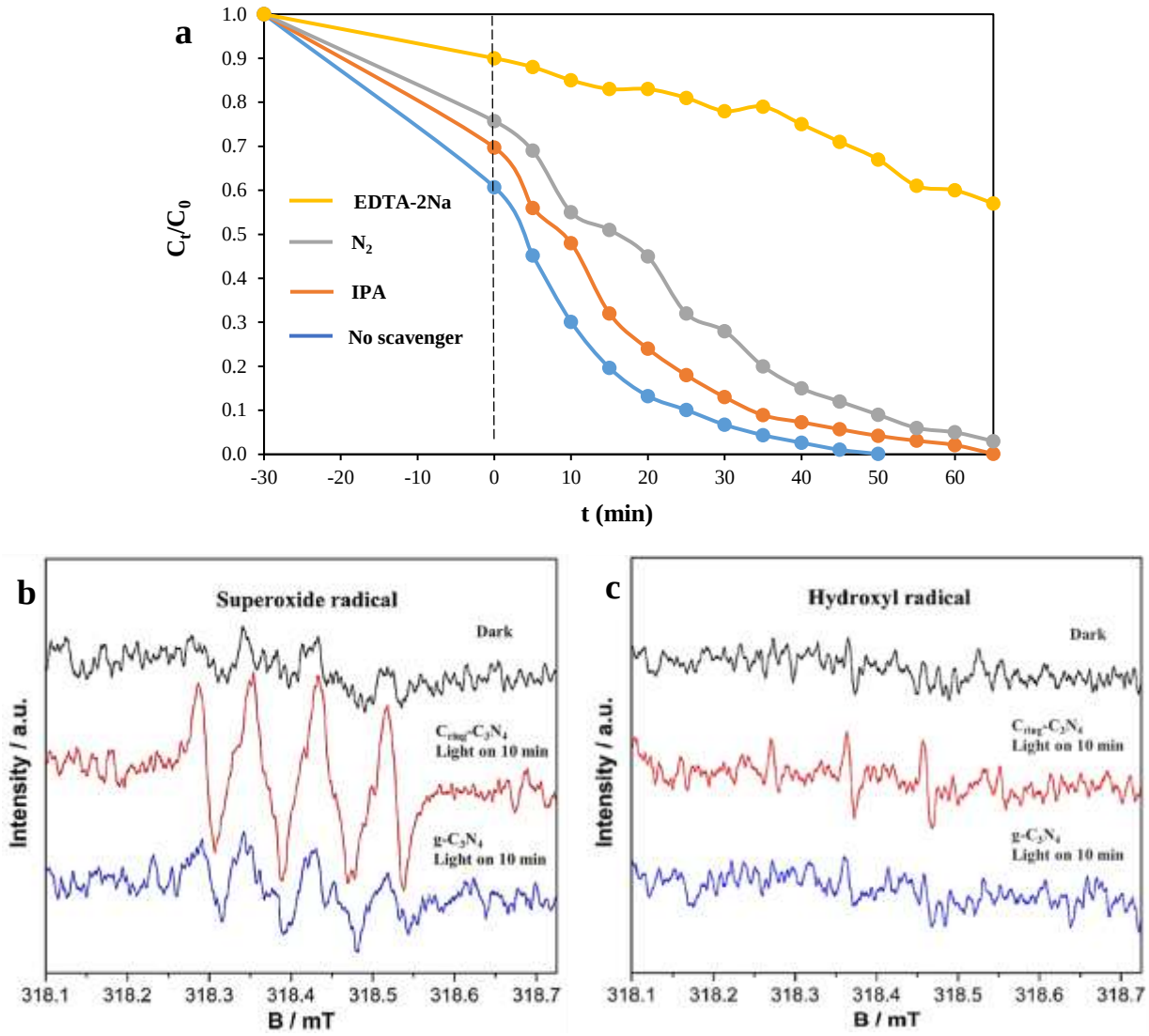

Figure S9. (**a**), MB over C_{ring}-C_3N_4 in the presence of Na_2EDTA, IPA, N_2 and in the absence of scavengers; (**b**), ESR spectra of DMPO-$O_2^{\cdot-}$ for C_{ring}-C_3N_4 and bulk g-C_3N_4; (**c**), ESR spectra of DMPO-$^{\cdot}$OH for C_{ring}-C_3N_4 and bulk g-C_3N_4.

Figure S10. Picture of the employed photo-reactor for photoreduction of CO_2 to CH_4.

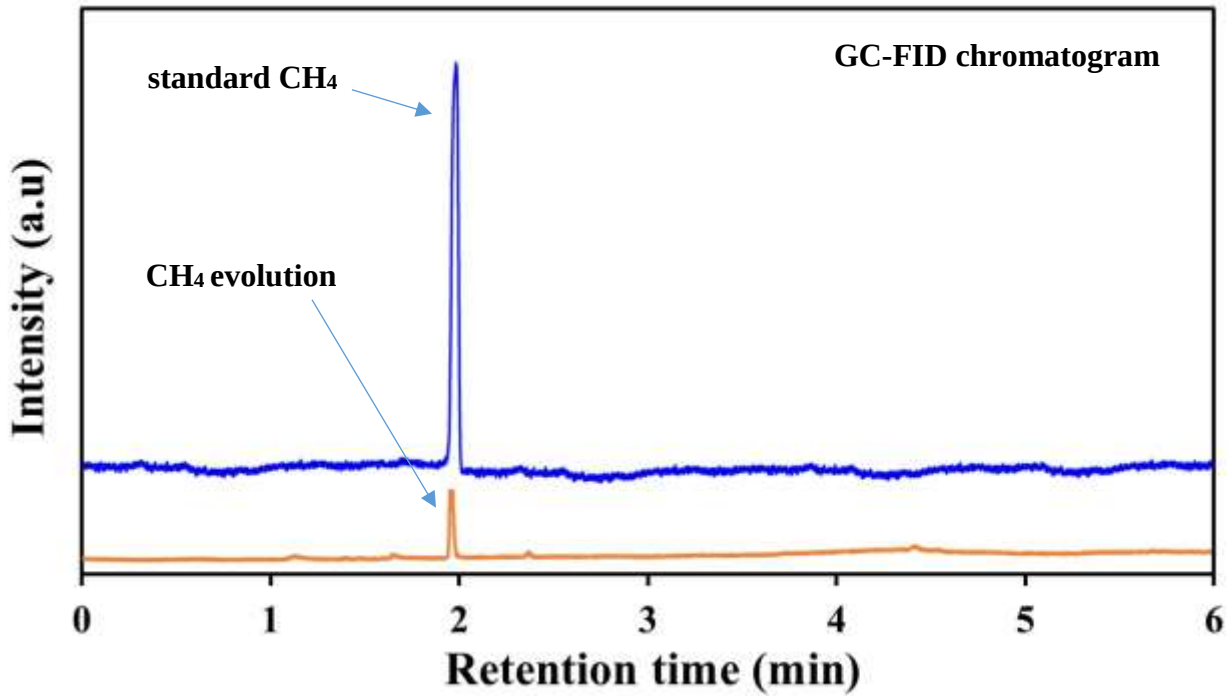

Figure S11. The chromatogram of the standard methane sample and the reaction mixture.

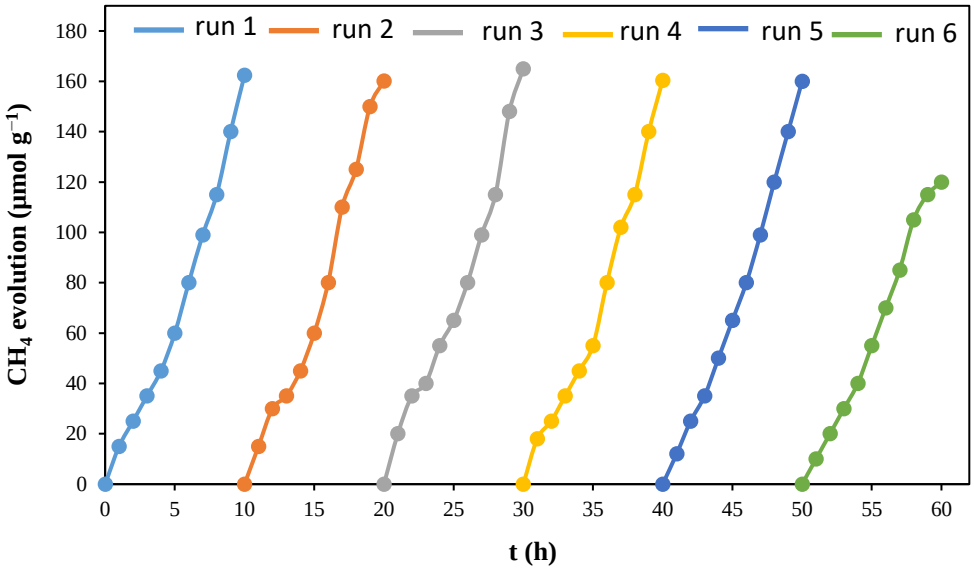

Figure S12. Reusability study of C_{rng}-C_3N_4 in the photocatalytic conversion of CO_2 to CH_4.

Calculation of AQY:
Photocatalytic reaction with C_{ring}-C_3N_4 nanosheet photocatalyst from [1]:

Main product: CH_4
Reactor type: Batch circulation water reactor (pyrex tubular reactor)
Product yield: 162.4 μmol g_{cat}^{-1} after 10 h
Apparent light input (H): 438 mW/cm^2
Area of irradiation (A): computed from tubular reactor dimensions
(length: 10.0 cm × diameter: 6.0 cm) A = 0.006 m^2
Band gap: 2.7 eV

The number of reacted electrons is computed by:

$$\text{Number of reacted electrons } = \begin{bmatrix}\text{mol of product}\\ \text{produced in time, t}\end{bmatrix} * \begin{bmatrix}\text{Number of electrons}\\ \text{required to produce}\\ \text{1 mol of product}\end{bmatrix} * \mathrm{N_A}$$

Since $CO_2 + 8H^+ + 8e^- \rightarrow CH_4 + 2H_2O$, it requires 8 electrons to produce 1 mole of CH_4 as the product

$$\text{Number of reacted electrons} = \left[\frac{162.4 * 10^{-6}}{10}\ \frac{\text{mol}}{\text{g h}}\right] * [8] * 6.022 * 10^{23}$$

$$\text{Number of reacted electrons} = 7.82 * 10^{19}$$

The number of incident photons is computed by:

$$\text{Effective number of incident photons} = \left[\frac{\text{Light absorbed by the photocatalyst}}{\text{Average photon energy}}\right] * \mathrm{t}$$

where

$$\text{Light absorbed by the photocatalyst} = \mathrm{H} * \mathrm{A} = 43.8\ \frac{\mathrm{w}}{\mathrm{m^2}} * 0.006\ \mathrm{m^2} = 0.2628\ \mathrm{W}$$

$$\text{Average photon energy} = \frac{\mathrm{hC}}{\lambda}$$

And, λ is the average wavelength of the absorption range of the photocatalyst. The maximum wavelength from the band gap is computed by:

$$\lambda_{max} = \frac{hC}{E_g} = \frac{(6.626 * 10^{-34}\, j.s) * (3 * 10^8\, m/s)}{2.7\ \text{eV}} * \frac{1\ \text{eV}}{1.6\ * 10^{-19}\, j} * 10^9 = 460.1\ \text{nm}$$

Therefore, the average wavelength would be:

$$\lambda = \frac{\lambda_{min} + \lambda_{max}}{2} = \frac{250 + 460.1}{2} = 355.05$$

The average photon energy is then computed to be:

$$\text{Average photon energy} = \frac{(6.626 * 10^{-34}\, j.s) * (3 * 10^8\, m/s)}{355.05 * 10^{-9}\, m} = 5.6 * 10^{-19}$$

$$\text{Effective number of incident electrons} = \left[\frac{0.2628\ \text{W}}{5.6 * 10^{-19}\, j}\ \frac{3600\ \text{s}}{1\ \text{h}}\right] = 1.689 * 10^{21}$$

AQY calculation:

$$\text{AQY (\%)} = \left[\frac{\text{number of reacted electrons}}{\text{Effective number of incident electrons}}\right] * 100$$

$$\text{AQY (\%)} = \left[\frac{7.82 * 10^{19}}{1.689 * 10^{21}}\right] * 100 = 4.63\ \%$$

Photocatalytic reaction with bulk g-C_3N_4 photocatalyst:

Reactor type: Batch circulation water reactor (pyrex tubular reactor)
Product yield: 6.875 μmol g_{cat}^{-1} after 10 h
Apparent light input (H): 438 mW/cm^2
Area of irradiation (A): computed from tubular reactor dimensions
(length: 10.0 cm × diameter: 6.0 cm) A = 0.006 m^2
Band gap: 2.7 eV

The number of reacted electrons is computed by:

$$\text{Number of reacted electrons } = \begin{bmatrix} \text{mol of product} \\ \text{produced in time, t} \end{bmatrix} * \begin{bmatrix} \text{Number of electrons} \\ \text{required to produce} \\ \text{1 mol of product} \end{bmatrix} * N_A$$

Since $CO_2 + 8H^+ + 8e^- \rightarrow CH_4 + 2H_2O$, it requires 8 electrons to produce 1 mole of CH_4

$$\text{Number of reacted electrons} = \left[\frac{6.875 * 10^{-6}}{10} \frac{\text{mol}}{\text{g h}}\right] * [8] * 6.022 * 10^{23}$$

$$\text{Number of reacted electrons} = 3.3121 * 10^{18}$$

The number of incident photons is computed by:

$$\text{Effective number of incident photons} = \left[\frac{\text{Light absorbed by the photocatalyst}}{\text{Average photon energy}}\right] * t$$

Wherein light absorbed by the photocatalyst and average photon energy is found to be:

$$\text{Light absorbed by the photocatalyst} = H * A = 43.8 \frac{w}{m^2} * 0.006\ m^2 = 0.2628\ W$$

$$\text{Average photon energy} = \frac{hC}{\lambda}$$

where λ is the average wavelength of the absorption range of the photocatalyst. The maximum wavelength from the band gap was computed by:

$$\lambda_{max} = \frac{hC}{E_g} = \frac{(6.626 * 10^{-34}\ j.s) * (3 * 10^8\ m/s)}{2.7\ eV} * \frac{1\ eV}{1.6\ * 10^{-19}\ j} * 10^9 = 460.1\ nm$$

Therefore, the average wavelength would be

$$\lambda = \frac{\lambda_{min} + \lambda_{max}}{2} = \frac{250 + 460.1}{2} = 355.05$$

The average photon energy is then computed to be

$$\text{Average photon energy} = \frac{(6.626 * 10^{-34}\ \text{j.s}) * (3 * 10^{8}\ \text{m/s})}{355.05 * 10^{-9}\ \text{m}} = 5.6 * 10^{-19}$$

$$\text{Effective number of incident electrons} = \left[\frac{0.2628\ \text{W}}{5.6 * 10^{-19}\ j}\ \frac{3600\ \text{s}}{1\ \text{h}}\right] = 1.689 * 10^{21}$$

AQY calculation:

$$\text{AQY (\%)} = \left[\frac{\text{number of reacted electrons}}{\text{Effective number of incident electrons}}\right] * 100$$

$$\text{AQY (\%)} = \left[\frac{3.3121 * 10^{18}}{1.689 * 10^{21}}\right] * 100 = 0.1961\ \%$$

$$\left[\frac{\text{AQY (\%) } C_{ring} - C_3N_4}{\text{AQY (\%) g} - C_3N_4}\right] = \left[\frac{4.63}{0.1961}\right] = 23.61$$

Table S1. Linear and nonlinear equations of absorption isotherms.

Name of models isotherm	Equations	Plots for isotherms
Linear adsorption isotherms		
Langmuir model [1]	$\frac{C_e}{Q_e} = \frac{1}{Q_m} C_e + \frac{1}{k_L Q_m}$	$\frac{C_e}{Q_e}$ *vs.* C_e
Freundlich model [2]	$\ln q_e = \ln k_f + \frac{1}{n} \ln C_e$	$\ln Q_e$ *vs.* $\ln C_e$
Temkin model [3]	$Q_e = \left(\frac{RT}{b}\right) \ln k_T + \left(\frac{RT}{b}\right) \ln C_e$ $B_T = \frac{RT}{b}$	Q_e *vs.* $\ln C_e$
Dubinin-radushkevich model [3]	$ln\, Q_e = \ln Q_m - \beta\varepsilon^2$ $E = \frac{1}{\sqrt{(-2\beta)}}$ $\varepsilon = RT \ln\left(1 + \frac{1}{C_e}\right)$	$ln\, Q_e$ *vs.* ε^2
Nonlinear adsorption isotherms		
Langmuir model [1]	$Q_e = Q_m k_L \frac{C_e}{1 + k_L C_e}$	Q_e *vs.* C_e
Freundlich model [2]	$Q_e = k_f C_e^{\frac{1}{n}}$	Q_e *vs.* C_e
Temkin model [3]	$Q_e = \frac{RT}{b} (ln\, k_T C_e)$ $B_T = \frac{RT}{b}$	Q_e *vs.* C_e
Dubinin-radushkevich model [3]	$Q_e = q_m\, e^{-\beta\varepsilon^2}$	Q_e *vs.* C_e

Table S2. Linear and nonlinear equations of kinetic isotherms.

Name of models isotherm	Equations	Plots for isotherms
linear kinetic isotherms		
Pseudo-first-order model [4]	$ln\ (Q_e - Q_t) = \ln Q_e - tk_1$	$ln\ (Q_e - Q_t)$ *vs.* t
Pseudo-second-order model [5]	$\frac{t}{Q_t} = \frac{1}{k_2 Q_e^2} + \frac{t}{Q_e}$	$\frac{t}{Q_t}$ *vs.* t
Elovich model [6]	$Q_t = \frac{1}{\beta} \ln\ (\alpha\beta) + \frac{1}{\beta}\ ln\ t$	Q_t *vs.* $ln\ t$
Intraparticle diffusion model [7]	$Q_t = k_{id} t^{\frac{1}{2}} + k_0$	Q_t *vs.* $t^{\frac{1}{2}}$
Nonlinear kinetic isotherms		
Pseudo-first-order model [4]	$Q_t = Q_e(1 - \exp - kt)$	Q_t *vs.* t
Pseudo-second-order model [5]	$Q_t = \frac{k_2 Q_e^2 t}{1 + k_2 Q_e t}$	Q_t *vs.* t
Elovich model [6]	$Q_t = \beta \ln (\alpha\beta t)$	Q_t *vs.* t
Intraparticle diffusion model [7]	$Q_t = k_{id} t^{\frac{1}{2}} + k_0$	Q_t *vs.* t

Table S3. Anova and Akaike information criterion tests for linear kinetic and adsorption isotherms.

Adsorption isotherm	Sum Sq	Sum Sq Error	Mean Sq	Mean Sq Error	F	P_{value}	ACI
Langmuir	6.9×10^{-2}	5.3×10^{-4}	6.9×10^{-2}	8.89×10^{-5}	783.24	1.4×10^{-7}	−22.1812
Freundlich	1.35	5.3×10^{-2}	1.35	8.98×10^{-3}	152.23	1.7×10^{-5}	−6.1914
Temkin	5309.6	690.11	5309.6	115.02	46.16	4.9×10^{-4}	26.7114
Dubinin-radushkevich	1.03	0.37	1.03	6.3×10^{-2}	16.45	6.7×10^{-3}	0.593
Kinetics modeling							
Pseudo first order	9.42	8.9×10^{-2}	9.42	1.3×10^{-2}	738.91	2.3×10^{-8}	−5.447
Pseudo second order	0.31	3.8×10^{-2}	3.1×10^{-1}	5.5×10^{-3}	56.32	1.4×10^{-4}	−8.7281
Elovich	12295	259.14	12295	37.02	332.11	3.7×10^{-7}	25.7218
Intraparticle diffusion	5666.7	333.08	5666.7	55.51	102.08	5.5×10^{-5}	26.8826

Table S4. A comparison between the various photocatalysts for photoreduction of CO_2 to CH_4.

Photocatalyst	CH_4 Yield (μmol/g h)	Light input (W/m^2)	Area of irradiation (m^2)	Band gap (eV)	Wavelength (nm)		Ave. λ (nm)	No. of reacted electrons	Average photon energy (J)	No. of incident photons	AQY (%)
					λmin	λmax					
Pt-XG/RBT [8]	37	1000	0.00049	2.41	250	515.5	383	1.78×10^{20}	5.19×10^{-19}	3.4×10^{21}	5.2479
C,N-TNT06 [9]	9.75	1000	0.00071	2.8	250	443.7	347	4.7×10^{19}	5.73×10^{-19}	4.46×10^{21}	1.0532
In_2O_3–C_3N_4 [10]	7.991	12000	0.00063	2.8	250	444	347	3.85×10^{19}	5.73×10^{-19}	4.71×10^{21}	0.082
CZTS-ZnO [11]	0.095	1000	0.00041	1.74	250	714	482	4.58×10^{17}	4.12×10^{-19}	3.58×10^{21}	0.0128
HCP-TiO_2-FG [12]	27.62	4330	0.00031	2.34	420	531	475	1.33×10^{20}	4.18×10^{-19}	1.17×10^{22}	1.14
Pd_xCu_1-TiO_2 [13]	19.6	20	0.0064	-	250	400	325	9.44×10^{19}	6.12×10^{-19}	7.53×10^{20}	12.53
Pt-X-RT [14]	1.13	1000	0.00071	2.85	250	435.9	343	5.44×10^{18}	5.8×10^{-19}	4.41×10^{21}	0.1234
Pt/TiO_2 [15]	2.85	348	0.0084	3.18	250	391	320	1.37×10^{19}	6.21×10^{-19}	1.69×10^{22}	0.081
Cu_xO−TiO_2 [16]	0.152	1000	0.00071	3.15	250	394.4	322	7.32×10^{17}	6.17×10^{-19}	4.14×10^{21}	0.0177
C_{ring}-C_3N_4 In this work	16.24	43.8	0.006	2.7	250	460.1	355.05	7.82×10^{19}	5.6×10^{-19}	1.689×10^{21}	4.63

Table S5. The comparison of the synthesized photocatalyst with some literature-reported photocatalysts in term of their ability for degradation of Methylene blue.

Photocatalyst	**$W_{Catalyst}$ (g)**	**Volume and concentration of MB**	**Irradiation Time (h)**	**mg MB/$W_{Catalyst}$**	**Degradation efficiency[a]**	**Reference**
Nanoporous Graphitic Carbon Nitride	0.025	50 mL 10 mg/L	3	20	0.11	[17]
TiO_2 nano-sized particles	1	600 mL 20 mg/L	9	12	0.02	[18]
TiO_2/ZnO	0.3	10 mL 10 mg/L	5	0.3	0.001	[19]
Al_2O_3/Fe_2O_3	0.2	100 mL 25 mg/L	1.5	12.5	0.14	[20]
Fe_3O_4@rGO@ TiO_2	0.05	50 mL 10 mg/L	2	10	0.08	[21]
TiO_2/polyacryl amide	0.025	25 mL 10 mg/L	5	10	0.03	[22]
SnO_2/S-doped g-C_3N_4	0.14	500 mL 6 mg/L	2.5	21.4	0.14	[23]
Ag/g-C_3N_4	0.1	300 mL 10 mg/L	1	30	0.5	[24]
C_3N_4/ZnO	0.15	150 mL 3.2 mg/L	2	3.2	0.03	[25]
npg-C_3N_4	0.001	20 mL 20 mg/L	0.75	400	8.9	[26]
C_{ring}-C_3N_4	0.004	40 mL 20 mg/L	0.75	200	4.4	This work

[a]Degradation efficiency was defined as (mg MB/$W_{Catalyst}$) per minute of the irradiation time in this table.

References

(1) Hallajiqomi, M.; Eisazadeh, H., Adsorption of manganese ion using polyaniline and it's nanocomposite: Kinetics and isotherm studies. *J. Ind. Eng. Chem.* **2017**, 55, 191-197.

(2) Araújo, C. S.; Almeida, I. L.; Rezende, H. C.; Marcionilio, S. M.; Léon, J. J.; de Matos, T. N., Elucidation of mechanism involved in adsorption of Pb (II) onto lobeira fruit (Solanum lycocarpum) using Langmuir, Freundlich and Temkin isotherms. *Microchem. J.* **2018**, 137, 348-354.

(3) Dada, A.; Olalekan, A.; Olatunya, A.; Dada, O., Langmuir, Freundlich, Temkin and Dubinin–Radushkevich isotherms studies of equilibrium sorption of Zn^{2+} unto phosphoric acid modified rice husk. IOSR-JAC. **2012**, 3, 38-45.

(4) Badawi, M.; Negm, N.; Abou Kana, M.; Hefni, H.; Moneem, M. A., Adsorption of aluminum and lead from wastewater by chitosan-tannic acid modified biopolymers: isotherms, kinetics, thermodynamics and process mechanism. *Int. J. Biol. Macromol*. **2017**, 99, 465-476.

(5) Tan, K.; Hameed, B., Insight into the adsorption kinetics models for the removal of contaminants from aqueous solutions. *J. Taiwan Inst. Chem. Eng.* **2017**, 74, 25-48.

(6) Cheung, C. W.; Porter, J. F.; McKay, G., Elovich equation and modified second-order equation for sorption of cadmium ions onto bone char. *J. Chem. Technol. Biotechnol.* **2000**, 75, 963-970.

(7) Aljeboree, A. M.; Alkaim, A. F.; Al-Dujaili, A. H., Adsorption isotherm, kinetic modeling and thermodynamics of crystal violet dye on coconut husk-based activated carbon. *Desalin Water Treat.* **2015**, 53, 3656-3667.

(8) Sorcar, S.; Thompson, J.; Hwang, Y.; Park, Y. H.; Majima, T.; Grimes, C. A.; Durrant, J. R.; In, S.-I., High-rate solar-light photoconversion of CO_2 to fuel: controllable transformation from C1 to C2 products. *Energy Environ. Sci.* **2018**, 11, 3183-3193.

(9) Parayil, S. K.; Razzaq, A.; Park, S.-M.; Kim, H. R.; Grimes, C. A.; In, S.-I., Photocatalytic conversion of CO_2 to hydrocarbon fuel using carbon and nitrogen co-doped sodium titanate nanotubes. *Appl. Catal., A.* **2015**, 498, 205-213.

(10) Cao, S.-W.; Liu, X.-F.; Yuan, Y.-P.; Zhang, Z.-Y.; Liao, Y.-S.; Fang, J.; Loo, S. C. J.; Sum, T. C.; Xue, C., Solar-to-fuels conversion over In_2O_3/g-C_3N_4 hybrid photocatalysts. *Appl. Catal., B.* **2014**, 147, 940-946.

(11) Zubair, M.; Razzaq, A.; Grimes, C. A.; In, S.-I., Cu_2ZnSnS_4 (CZTS)-ZnO: A noble metal-free hybrid Z-scheme photocatalyst for enhanced solar-spectrum photocatalytic conversion of CO_2 to CH_4. *J. CO2 Util.* **2017**, 20, 301-311.

(12) Wang, S.; Xu, M.; Peng, T.; Zhang, C.; Li, T.; Hussain, I.; Wang, J.; Tan, B., Porous hypercrosslinked polymer-TiO_2-graphene composite photocatalysts for visible-light-driven CO_2 conversion. *Nat. Commun.* **2019**, 10, 1-10.

(13) Long, R.; Li, Y.; Liu, Y.; Chen, S.; Zheng, X.; Gao, C.; He, C.; Chen, N.; Qi, Z.; Song, L., Isolation of Cu atoms in Pd lattice: forming highly selective sites for photocatalytic conversion of CO_2 to CH_4. *J. Am. Chem. Soc.* **2017**, 139, 4486-4492.

(14) Razzaq, A.; Sinhamahapatra, A.; Kang, T.-H.; Grimes, C. A.; Yu, J.-S.; In, S.-I., Efficient solar light photoreduction of CO_2 to hydrocarbon fuels via magnesiothermally reduced TiO_2 photocatalyst. *Appl. Catal., B.* **2017**, 215, 28-35.

(15) Li, X.; Zhuang, Z.; Li, W.; Pan, H., Photocatalytic reduction of CO_2 over noble metal-loaded and nitrogen-doped mesoporous TiO_2. *Appl. Catal., A.* **2012**, 429, 31-38.

(16) Park, S.-M.; Razzaq, A.; Park, Y. H.; Sorcar, S.; Park, Y.; Grimes, C. A.; In, S.-I., Hybrid Cu_xO–TiO_2 Heterostructured Composites for Photocatalytic CO_2 Reduction into Methane Using Solar Irradiation: Sunlight into Fuel. *ACS Omega.* **2016**, 1, 868-875.

(17) Xu, J.; Wang, Y.; Zhu, Y., Nanoporous graphitic carbon nitride with enhanced photocatalytic performance. *Langmuir.* **2013**, 29, 10566-10572.

(18) Dariani, R.; Esmaeili, A.; Mortezaali, A.; Dehghanpour, S., Photocatalytic reaction and degradation of methylene blue on TiO_2 nano-sized particles. *Optik.* **2016**, 127, 7143-7154.

(19) Chekir, N.; Benhabiles, O.; Tassalit, D.; Laoufi, N. A.; Bentahar, F., Photocatalytic degradation of methylene blue in aqueous suspensions using TiO_2 and ZnO. *Desalin Water Treat.* **2016**, 57, 6141-6147.

(20) Singh, A.; Khare, P.; Verma, S.; Bhati, A.; Sonker, A. K.; Tripathi, K. M.; Sonkar, S. K., Pollutant Soot for Pollutant Dye Degradation: Soluble Graphene Nanosheets for Visible Light Induced Photodegradation of Methylene Blue. *ACS Sustainable Chem. Eng*. **2017**, 5, 8860-8869.

(21) Yang, X.; Chen, W.; Huang, J.; Zhou, Y.; Zhu, Y.; Li, C., Rapid degradation of methylene blue in a novel heterogeneous Fe_3O_4@rGO@TiO_2-catalyzed photo-Fenton system. *Sci. Rep*. **2015**, 5, 10632.

(22) Kazemi, F.; Mohamadnia, Z.; Kaboudin, B.; Karimi, Z., Photodegradation of methylene blue with a titanium dioxide/polyacrylamide photocatalyst under sunlight. *J. Appl. Polym. Sci*. **2016**, 133.

(23) Jourshabani, M.; Shariatinia, Z.; Badiei, A., In situ fabrication of SnO_2/S-doped g-C_3N_4 nanocomposites and improved visible light driven photodegradation of methylene blue. *J. Mol. Liq*. **2017**, 248, 688-702.

(24) Li, H.; Jing, Y.; Ma, X.; Liu, T.; Yang, L.; Liu, B.; Yin, S.; Wei, Y.; Wang, Y., Construction of a well-dispersed Ag/graphene-like g-C_3N_4 photocatalyst and enhanced visible light photocatalytic activity. *RSC Adv*. **2017**, 7, 8688-8693.

(25) Amornpitoksuk, P.; Suwanboon, S.; Sirimahachai, U.; Randorn, C.; Yaemsunthorn, K., Photocatalytic degradation of methylene blue by C_3N_4/ZnO: the effect of the melamine/ZnO ratios. *Bull. Mater. Sci*. **2016**, 39, 1507-1513.

(26) Ashrafi, H., Akhond, M., Absalan, G. Adsorption and photocatalytic degradation of aqueous methylene blue using nanoporous carbon nitride. *J. Photochem. Photobiol., A.* **2020**, 396, 112533.